

Anticancer Activities of Re(I) Tricarbonyl and Its Imidazole-Based Ligands: Insight from a Theoretical Approach

Mabu L. Matlou, Hitler Louis, Destiny E. Charlie, Ernest C. Agwamba, Ismail O. Amodu, Vuyelwa J. Tembu, and Amanda-Lee E. Manicum*



Cite This: *ACS Omega* 2023, 8, 10242–10252



Read Online

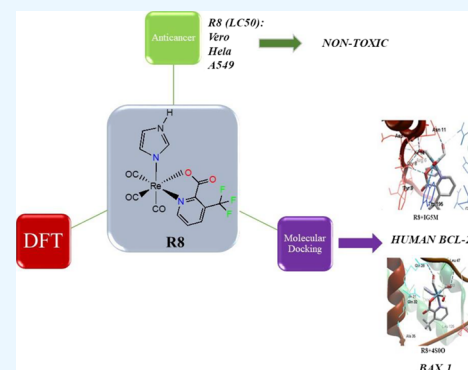
ACCESS |

Metrics & More

Article Recommendations

Supporting Information

ABSTRACT: Rhenium complexes have been observed experimentally to exhibit good inhibitory activity against malignant cells. Hence, our motivation is to explore this activity from a theoretical perspective. In the present study, density functional theory (DFT) and in silico molecular docking approaches were utilized to unravel the unique properties of metal-based rhenium tricarbonyl complexes as effective anticancer drugs. All DFT calculations and geometric optimizations were conducted using the well-established hybrid functional B3LYP-GD(BJ)/Gen/6-311++G(d,p)/LanL2DZ computational method. The FT-IR spectroscopic characterization of the complexes: *fac*-[Re(Pico)(CO)₃(Pz)] (R1), *fac*-[Re(Pico)(CO)₃(Py)] (R2), *fac*-[Re(Dfpc)(CO)₃(H₂O)] (R3), *fac*-[Re(Dfpc)(CO)₃(Pz)] (R4), *fac*-[Re(Dfpc)(CO)₃(Py)] (R5), *fac*-[Re(Tfpc)(CO)₃(H₂O)] (R6), *fac*-[Re(Tfpc)(CO)₃(Py)] (R7), and *fac*-[Re(Tfpc)(CO)₃(Im)] (R8) was explored. To gain insights into the electronic structural properties, bioactivity, and stability of these complexes, the highest occupied molecular orbital–lowest unoccupied molecular orbital analysis, binding energy, and topological analysis based on quantum theory of atoms-in-molecules were considered. The anticancer activities of the complexes were measured via in silico molecular docking against human BCL-2 protein (IG5M) and proapoptotic (agonist) BAX 1 protein (450O). The results showed that the studied complexes exhibited good binding affinity (−3.25 to −10.16 kcal/mol) and could cause significant disruption of the normal physiological functions of the studied proteins. The results of DFT calculations also showed that the studied complexes exhibited good stability and are suitable candidates for the development of anticancer agents.



1. INTRODUCTION

The quest or pursuit for a new and more effective anticancer drug has been highly significant in the medical world. Several breakthroughs were obtained while studying metal-based complexes as anticancer therapeutics in cancer treatment.¹ This success is exemplified by the discovery of cisplatin in 1960 by Barnett Rosenberg.² Significantly, it has also conceptualized the modern era of metal-based anticancer drugs, like cisplatin, carboplatin, and oxaliplatin.^{3,4} In recent years, investigations were carried out with the commitment of researchers and scientists to develop a new anticancer drug consisting of a range of different complexes emanating from Re, Au, Pd, Rh, Os, and Ir metal complexes.^{5–7} The efficiency of metal-based drugs in cancer therapy cannot be underestimated, as it has recently been used in about 32 out of 78 cancer regimens.⁸ Despite these spectacular attributes found in metal-based complexes, they have certain disadvantages as it causes toxic side effects and displays chemotherapeutic resistance.^{9,10} Various studies on the transition metal rhenium (Re) have been conducted in recent years to develop novel anticancer agents.^{11–13} Syntheses were carried out on many rhenium complexes, exploring their potential properties as an anticancer agent due to their biological activity of cytotoxicity.¹⁴ The

potential of rhenium complexes was first identified in tricarbonyl bisimine complexes in the HeLa cells.¹⁵ Rhenium is more economically feasible; hence, all center of attention has been conveyed to these significant Re(I) tricarbonyl complexes applied as a cancer drug in therapeutics.^{16,17} Upon investigations on vast numbers of rhenium compounds with higher oxidation states, alongside hetero-metallic complexes, researchers have given little attention to Re(I) tricarbonyl complexes.¹⁸ These compounds were observed to possess anticancer characteristics of a chemotherapeutic drug and phytophysical properties.¹⁴ Research has proven that rhenium complexes possess cytotoxic and phototoxic properties against malevolent/malignant cells.¹⁹ Evidently, all rhenium complexes are still undergoing clinical investigations to prove their full potential as an anticancer drug, whereas many more are still awaiting ethical approval to be clinically proven.^{20,21} There are

Received: December 6, 2022

Accepted: January 26, 2023

Published: March 7, 2023



limited reports of Re(I) tricarbonyl complexes of lipophilic phenanthroline derivatives of rhenium complexes as a potential anticancer agent.

The use of density functional theory (DFT), molecular docking, and dynamic simulation have recently gained much attention in drug design due to their proven ease and detailed revelation in drug and receptor protein reactivity and interactions.^{22–26} This approach has become vital in catalyzing cancer research, and the need has become too necessary to overemphasize, consequently, giving rise to peculiarity and urgency in cancer malignant management.²⁷ Recent studies have adopted the computer-aided drug design approach to study the antineoplastic activities of novel molecules. These have accelerated the discovery of a more potent pharmacotherapeutic agent and created a platform for further clinical trials.^{28,29} Applying the first-principles DFT and molecular docking, scientists were able to investigate *N*-(1*H*-pyrrol-2-yl)methylene)-4-methylaniline as a future chemotherapeutic medication for the treatment of castration-resistant prostate cancer (CRPC).^{26,30} Another investigation by Eno et al.²⁴ adopted a similar approach to study the electronic structure properties and antineoplastic potential of the 6-methylpyridine-2-carbaldehyde-*N*-(4)-ethylthiosemicarbazone and its platinum(II) and zinc(II) complexes, with promising results. Azo-based dyes also were extensively investigated for their unique biological activity, especially as chemotherapeutic agents in malignant glioblastoma management.³¹

Furthermore, Khattab and Al-Karmalawy utilized the DFT calculations and molecular docking to investigate the activity of some nocodazole analogues, including mebendazole, albendazole, oxfendazole, nocodazole, flubendazole, oxibendazole, bendazole, fenbendazole, ciclobendazole, and thiabendazole as a potential anticancer drug. Flubendazole was achieved as a promising anticancer candidate.³² Al-Otaibi and co-workers adopted the DFT study and molecular docking analysis approach to investigate Bendamustine's spectroscopic, quantum mechanical, and electronic excitation properties (ethanol solvent) as an anticancer drug.³³ Hence, it will not be out of place if a similar approach is applied in the current study of rhenium complexes, which has already revealed some level of biological activity of cytotoxicity in the HeLa cells line as reflected by their growth inhibitory effects.²⁵ Rhenium carbonyl complexes with the *fac*-[Re(CO)₃]⁺ core bounded to a diimine bidentate ligand in the form of functionalized 2,2'-bipyridine (bipy) and 1,10-phenanthroline have revealed highly biological activity against cancer cells, which is more in the neutral and lipophilic phenanthroline derivatives of rhenium complexes.^{34,35}

Despite many experimental investigations on rhenium complexes, very limited literature is available on the investigation of rhenium complexes, especially the picolinic acid derivatives by the molecular modeling approach, like atomistic simulation using DFT and *in silico* molecular docking and molecular dynamic simulations. This investigation aims to further reveal their unique chemical quantum electronic structure properties, nature of interactions with amino acid residues, and stability of their complexes with proapoptotic (IG5M) and antiapoptotic proteins. Molecular properties derived from DFT computations are utilized to give the verdict on the stability and reactive nature of the complexes. The correlation between energy gap, second-order perturbation energy, and intermolecular charge transfer is considered and reported in detail. The studied complexes

were synthesized, characterized, and reported by Matlou et al.³⁶ They are designated as **R1–R8**. For comparison, the Dox ligand was utilized as the standard for the molecular docking experiments. Figure 1 shows the 2D diagrams of the studied metal complexes.

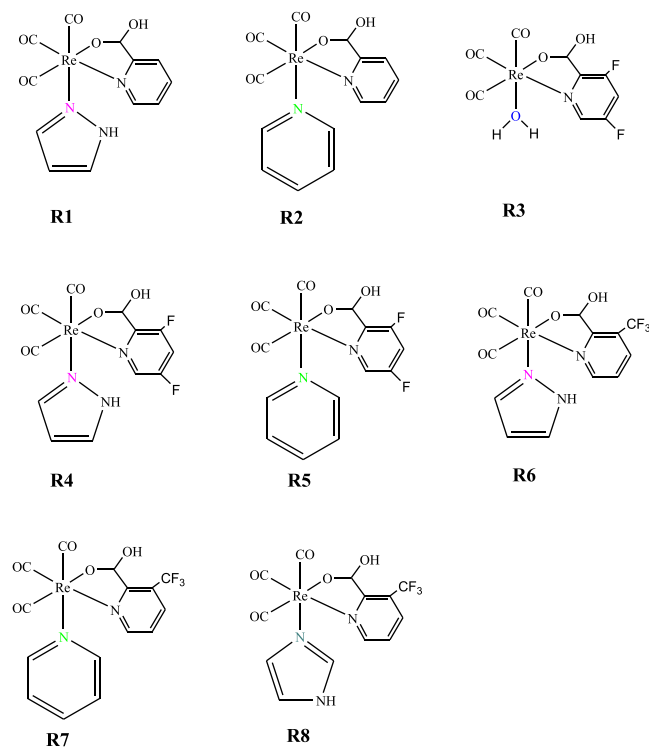


Figure 1. 2D representations of the studied Re(I) complexes.

2. METHOD

All complexes studied in this work were previously synthesized, characterized, and reported by Matlou et al.^{36–39}

2.1. Computational Details. **2.1.1. DFT Approach.** DFT has been utilized in geometric optimizations to ascertain minimum energy configurations and stable molecular geometries.^{40,41} This has been accomplished using a well-established DFT functional B3LYP/Gen by incorporating the empirical dispersion GD(BJ) as well as assigning the 6-311++G(d,p) and LanL2DZ basis set for lighter and heavy metal atoms, respectively.⁴¹ Investigations on all complexes have been carried out using frontier molecular orbital (FMO) or highest occupied molecular orbital (HOMO–LUMO) analysis, natural bonding orbital (NBO) analysis, binding energy, and quantum theory of atoms-in-molecules (QTAIM) analysis. Gaussian 16 software²⁴ was used to accomplish all computational calculations with its embedded GaussView 6.0.16 interface.⁴² The binding energy of each of the Rhenium complexes was obtained using eq 1:

$$E_{\text{int2}} = \left(E_{\text{comp}} - E_{\text{R1}} - E_{\text{R2}} - \frac{1}{2}E_{\text{M}} - E_{3\text{CO}} \right) - \left(E_{\text{comp}}^{\text{ZPE}} - E_{\text{R1}}^{\text{ZPE}} - E_{\text{R2}}^{\text{ZPE}} - \frac{1}{2}E_{\text{M}}^{\text{ZPE}} - E_{3\text{CO}} \right) \quad (1)$$

where the parameter E_{comp} signifies the energy of the complex, E_{R1} signifies the energy of fragment 1, E_{R2} represents the energy of fragment 2, $\frac{1}{2}E_{\text{M}}$ signifies the energy of the Rhenium

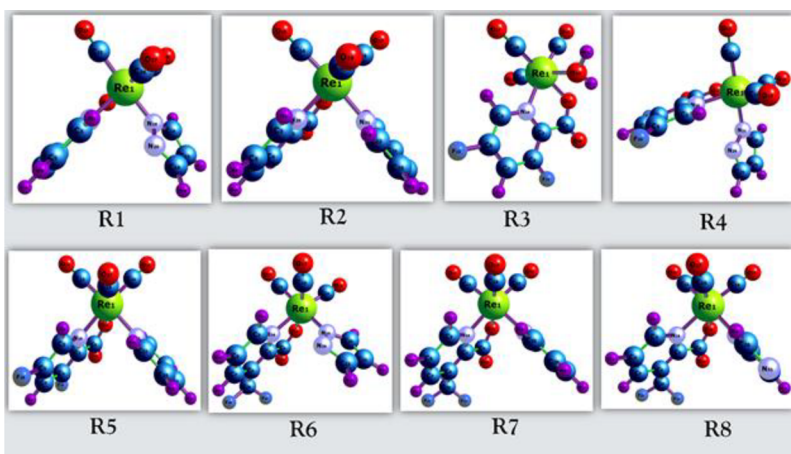


Figure 2. Optimized geometry of the studied metal complexes.

Table 1. Summary of the Spectroscopic Data for Complexes R1–R8

complexes	ν_{CO} (cm^{-1}) ³⁶	theory (cm^{-1})	λ_{max} (nm) ³⁶	ϵ ($\text{M}^{-1} \text{cm}^{-1}$) ³⁶
<i>fac</i> -[Re(Pico)(CO) ₃ (Pz)] (R1)	2028, 1926	2125	336	1835
<i>fac</i> -[Re(Pico)(CO) ₃ (Py)] (R2)	2024, 1911	2099	340	1667
<i>fac</i> -[Re(Dfpc)(CO) ₃ (H ₂ O)] (R3)	2035, 1869	2109	333	1893
<i>fac</i> -[Re(Dfpc)(CO) ₃ (Pz)] (R4)	2027, 1888	2066	338	1480
<i>fac</i> -[Re(Dfpc)(CO) ₃ (Py)] (R5)	2024, 1885	2102	330	1296
<i>fac</i> -[Re(Tfpc)(CO) ₃ (H ₂ O)] (R6)	2031, 1877	2064	333	2876
<i>fac</i> -[Re(Tfpc)(CO) ₃ (Py)] (R7)	2028, 1870	2101	330	1213
<i>fac</i> -[Re(Tfpc)(CO) ₃ (Im)] (R8)	2024, 1904	2098	337	1928

metal, $E_{3\text{CO}}$ represents the energy of three CO groups, $E_{\text{comp}}^{\text{ZPE}}$ is the zero point energy of the complex, $E_{\text{R1}}^{\text{ZPE}}$ is the zero point energy of fragment 1, $E_{\text{R2}}^{\text{ZPE}}$ is the zero point energy of fragment 2, $\frac{1}{2}E_{\text{M}}^{\text{ZPE}}$ represents the zero point energy of the Rhenium metal, and $E_{3\text{CO}}$ represents the zero point energy of three CO groups. Considering the second-order perturbation energies to arrive at a conclusion about stability and charge transfer mechanism, an NBO analysis was performed using NBO 3.1.⁴³ Information on the overall reactivity as well as the electronic structural properties of the studied molecules was derived from the quantum descriptors fundamentally obtained from the energy of the highest occupied molecular orbital (E_{HOMO}) and energy of the lowest unoccupied molecular orbital (E_{LUMO}), resulting in very useful descriptors such as the energy gaps and the global reactivity descriptors as postulated by generalized Koopmans' theorem.⁴⁴ The quantum chemical descriptors include Global softness (σ), chemical hardness (η), chemical potential (μ), and electrophilicity index (ω). More insights into intermolecular and intramolecular interactions of the studied complexes were obtained from the QTAIM, postulated by Richard F.W. Bader and his research team.⁶⁸ The optimized geometry of the studied complexes is depicted in Figure 2.

2.1.2. Molecular Docking Protocol. Cancer receptor protein isoform 1 of antiapoptotic human BCL-2 protein (1GSM)^{45,69} and autoinhibited Dimer of pro-apoptotic BAX I protein (4S0O)^{46,70} present in HeLa cell lines⁴⁷ was downloaded from RCSB PDB website.⁷¹ The proteins were prepared with Biovia discovery studio⁷² by removing all the water molecules, heteroatoms, and ligands. Then, the proteins were imported into Molegro Virtual Docker (MVD),⁷³ where the protein structure was mutated and optimized by adding the requisite charge and protonation to the faulty amino acid

residues. The molecular surface of the protein is created using the electrostatic surface type mapping, and a maximum of five (5) cavities was detected using expanded van der Waals force. Before importing the rhenium complex and doxorubicin (standard drug) as the ligand, the charge and flexible torsions were calculated, detected, and assigned by the MVD software algorithm. Furthermore, from the workspace, the following setting was used in the docking of the ligand and receptor protein by using the MolDock scoring (GRID) function with a grid resolution of 0.30 Å and a binding site with a radius of 15 Å with the center of point X:0.63, Y:−2.43, and Z:1.94. The internal electrostatic potential, internal H bond, and $\text{sp}^2\text{--sp}^2$ torsions were ignored. The MolDock SE search algorithm has a maximum number of 10 runs. The poses were constrained to the cavity, and energy minimization and H-bonds detected were optimized. The parameter settings were 1500 maximum iterations, with a population size of 50 energy threshold 100.00 kcal mol^{−1}, maximum step of 300, and neighbor distance factor of 1.00 Å. The docking was performed in a separate process by creating a script that executes in an external phase. The best pose was selected based on MolDock Score and recorded.

3. RESULTS AND DISCUSSION

3.1. Spectral Analysis. Comparatively, it is observed that the DFT stretching frequency values obtained for the eight complexes are in a close range to the experimental stretching frequency (Table 1).

3.2. Structural Parameters. Structural parameters such as bond lengths and angles were considered to characterize the bonding strength within the complex further. The bond length and angle were extracted for the R1 complex only, characterized as the most stable complex using crystal explorer. The bond angle equally gives information on the distribution

Table 2. Electronic Structural Properties of R1–R8 Complexes^a

compounds	E_{HOMO} (eV)	E_{LUMO}	E_{g} (eV)	σ	η	μ	ω	B.E. (eV)
R1	-6.6393	-2.5832	4.0561	0.2465	2.0281	-4.6112	5.2423	0.1888
R2	-6.3743	-2.4338	3.9405	0.2538	1.9702	-4.4040	4.9221	0.2130
R3	-6.9525	-3.0820	3.8706	0.2584	1.9353	-5.0172	6.5036	-198.299
R4	-6.8007	-2.9712	3.8295	0.2611	1.9147	-4.8859	6.2339	-198.347
R5	-6.5427	-2.8455	3.6972	0.2705	1.8486	-4.6941	5.9598	-198.323
R6	-6.7884	-2.9356	3.8529	0.2596	1.9264	-4.8620	6.1354	-336.946
R7	-6.5316	-2.7660	3.7655	0.2656	1.8828	-4.6488	5.7393	-336.922
R8	-7.0050	-3.0109	3.9941	0.2504	1.9971	-5.0080	6.2793	-337.606

^aHOMO–LUMO, energy gap, global softness (σ), chemical hardness (η), chemical potential (μ), electrophilicity index (ω), and binding energy.

of the bonding pair around the atoms. The complex was also obtained through geometric optimization and energy minimization to obtain a sensitive and stable system. The experimental and DFT structural parameters for the R1 complex are computed and presented in Tables S1 and S2 of the Supporting Information. The complex's experimental and DFT bond length values are observed to have slight variations, with a difference of about 0.03 Å. The bond of the Re atom to the six atoms surrounding it was obtained, and it is observed that the highest bond lengths are within, Re₁–N₁₈ (2.182 Å), Re₁–N₂₈ (2.179 Å), and Re₁–O₁₃ (2.146 Å), while the lowest is observed in Re₁–C₂₆ (1.926 Å), Re₁–C₂₄ (1.909 Å) and Re₁–C₂₂ (1.924 Å). The reasonably high bond length of 2.089 Å within Re₁–O₁₃ is a product of the increase in the density of electrons on the rhenium center arising from the monodentate sigma N/O-donor ligand, which increases π -back donation to the carbonyl and N–O bidentate ligands. This complex R1 exhibits hydrogen bonds in a one-dimensional chain, primarily formed through a bifurcate H-bond, existing between an N–H bond and two oxygen atoms in the acetate group. The bond angle portrayed some interesting characteristics as the bond angles are relatively close for all the values extracted. The highest bond angles were observed in C₂₂–Re₁–O₁₃ (94.64°), C₂₆–Re₁–N₁₈ (92.09°), and C₂₂–Re₁–C₂₄ (89.04°), and the lowest bond angle was observed in C₂₄–Re₁–C₂₆ (88.33°), N₁₈–Re₁–N₂₈ (85.91°), and N₂₈–Re₁–O₁₃ (75.90°). The slightest bond angle of the N–O to the rhenium center is because the bidentate N–O ligands bind strongly to the rhenium center see Figure 2.

3.3. Electronic Properties. **3.3.1. Reactivity Studies.** The highest occupied molecular orbital (HOMO) and the lowest unoccupied molecular orbital (LUMO) are the two grand parameters for which the global indices of reactivity are derived.⁴⁸ The change in energy between the HOMO and LUMO can be referred to as HOMO–LUMO energy gap, which is the lowest energy electronic excitation possible in a molecule.⁴⁹ When the mobility of the π electrons is greater in large conjugated π orbital systems, the energy distribution tends to be higher throughout the molecule. Fukui was the first to discover the critical role of the HOMO and LUMO in governing chemical reactions. The energy gap determines the kinetic stability and bioactivity of a molecule.^{50,51} The larger energy gap indicates low chemical reactivity, and the smaller energy gap exhibits high reactivity. Hence, the smaller the energy difference, the greater the reactivity and the lesser the stability of a complex.⁵¹ The energy of the HOMO and LUMO and their energy difference were computed to explore the chemical reactivity and stability and to estimate the quantum chemical descriptors of the rhenium complexes, respectively. The Gaussian 6.0.16 package, using DFT/B3LYP and the basic

set 6-311++G(d,p), has been employed in this investigation, as provided in Section 2.1 of the DFT computational details. Based on the generalized Koopmans's approximation, the quantum chemical descriptors such as band gap (E_{g}), global softness (σ), chemical hardness (η), chemical potential (μ), and electrophilicity index (ω) have been calculated by eqs 23456 and shown in Table 2.

$$E_{\text{g}} = E_{\text{HOMO}} + E_{\text{LUMO}} \quad (2)$$

$$\mu = -\chi = \frac{(E_{\text{HOMO}} + E_{\text{LUMO}})}{2} \quad (3)$$

$$\eta = \frac{E_{\text{HOMO}} - E_{\text{LUMO}}}{2} \quad (4)$$

$$\sigma = \frac{1}{2\eta} \quad (5)$$

$$\omega = \frac{\mu^2}{2\eta} \quad (6)$$

Also, the changes in the electronic structural properties of the studied complexes are obtained from the HOMO–LUMO analysis. The differences majorly influence this in the energy of the HOMO and LUMO aforementioned. The difference in energy between the two frontiers' molecular orbital can be used to predict the complex's energy, strength, reactivity, and stability after interaction.⁵² This reveals the change in electronic structural properties during the interaction of rhenium complexes with the cancer cell. From the result obtained in Table 2, the energy gaps of the complexes are observed to follow an increasing sequence of R5 < R7 < R4 < R6 < R3 < R2 < R8 < R1. From this trend, the least and most significant energy gaps are observed in R5 and R1 complexes with energy gap values of 3.6972 and 4.0561 eV, respectively. The least energy gap obtained for the R5 complex is due to the HOMO and LUMO energy values of -6.5427 and -2.8455 eV, respectively. The least energy gap of R5 suggests that R5 could be more reactive when compared with other complexes, based on the notion that molecular species with small energy gaps generally require a small amount of energy for electronic transitions from the HOMO to the LUMO, respectively. This ease of transition results in an increased in molecular reactivity as manifested by the second-order perturbation analysis. Also, the HOMO and LUMO energy values of -6.6393 and -2.5832 eV, respectively, are computed for the R1 complex. Also, one can observe from Table 2 that the energy gap value of 3.9941 eV for the R8 complex is very close to that obtained for the R1 complex ($E_{\text{g}} = 4.0561$ eV), with nearly insignificant decimal places high. This implies a charge transfer within the

Table 3. Second-Order Stabilization Energies and the Intermolecular Donor–Acceptor Natural Bonding Orbital and Other NBO Parameters of Most Interacting NBOs of the Complexes Obtained via NBO Analysis

compounds	donor NBO (<i>i</i>)	acceptor NBO (<i>j</i>)	E^2 (kcal/mol)	$E_{(i)} - E_{(j)}$	$F(I_j)$
R1	σ Re ₁ –N ₁₈	LP*Re ₁	92.94	0.03	0.136
R2	LP* Re ₁	σ^* Re ₁ –C ₁₈	88.67	0.09	0.153
R3	σ^* Re ₁ –C ₁₆	σ^* Re ₁ –C ₁₂	235.30	0.01	0.121
R4	LP O ₁₅	π^* Re ₁ –C ₁₄	96.79	0.29	0.211
R5	LP C ₃	π^* Re ₁ –N ₁₈	678.44	0.03	0.119
R6	LP O ₁₃	π^* Re ₁ –C ₁₂	94.76	0.29	0.211
R7	LP C ₂₈	π^* C ₂₅ –N ₃₄	132.24	0.09	0.114
R8	LP O ₁₃	π^* Re ₁ –C ₁₂	93.60	0.29	0.210

complex, which improves the bioactivity and ability to form biological interactions. This suggests that the strength and stability of the complex are determined by its increase in the energy gap between the HOMO and LUMO. At the same time, reactivity is realized by decreasing the energy gap values. Hence **R1** and **R8** complexes are the most stable and least reactive complexes, whereas the **R5** complex is the most reactive and least stable among the studied complexes interacting with the cancer cells. Note that the least stability of **R5** is the direct consequences of its small energy gap.

3.3.2. Binding Energy. Binding energy is usually referred to as the difference between the total energies of products and reactants.⁵³ It is the energy released due to bond formation and as a result of an interaction. From the calculated interaction energy of the complexes under study, as displayed in Table 3, slight variations in the values are observed between **R6**, **R7**, and **R8** complexes, as they have the highest binding energies of -336.946 , -336.922 , -337.606 a.u. respectively among the studied complexes. **R4** and **R5** complexes are observed with very close interaction energy values of -198.299 and -198.347 a.u., respectively. On the other hand, **R1** and **R2** complexes result in respective positive binding energy values of 0.1888 and 0.2130 a.u. The positive values of the two complexes **R1** and **R2** imply that the ligands consume higher energy only when the energy required is available. While the negative binding energy observed in the other eight complexes results from the consumption of minimal energy from the ligand. The more negative the binding energy, the greater the stability of the complex, and the more positive the binding energy of the complex, the lesser the stability of the complex.⁵⁴ Therefore, higher negative binding energy denotes better stability of the complex, thereby influencing the reactivity and potency of the drug. Comparatively, it is observed that the **R8** complex has the highest binding energy value of -337.606 a.u. The interaction energies of the studied complexes have been calculated via the Mathematical expression in eq 7:

$$E_{\text{int}} = (E_{\text{comp}} - E_{\text{R1}} - E_{\text{R2}} - E_{\text{M}} - 3\text{CO}) - (E_{\text{comp}}^{\text{ZPE}} - E_{\text{R1}}^{\text{ZPE}} - E_{\text{L2}}^{\text{ZPE}} - E_{\text{M}}^{\text{ZPE}} - 3\text{CO}) \quad (7)$$

where the various parameters of eq 7 have been carefully defined in Section 2.2.1 of the DFT computational section. The binding energy values obtained using this formula are shown in Table 3. Hence, it is deduced that the **R8** complex is the most stable complex, followed by **R7** and **R6** complexes due to their relatively closer and greatest binding/interaction energy values. This result agrees with that obtained in Section 3.3.1 of the reactivity studies.

3.3.3. Perturbation Theory Analysis. With maximum electron density in molecules, the natural bonding orbitals

(NBO) developed by Weinhold is a bonding orbital calculated to determine the electron density distribution in atoms and the bonds between interacting atoms.⁵⁵ The NBO analysis of compounds is an efficient tool for examining the intermolecular and intramolecular interactions resulting from chemical bonds that exist in molecules, aided by the information from the filled and vacant orbital.^{56,57} According to Weinhold's method, the NBO modeling divulges that when molecular orbitals are properly oriented, hyperconjugation confers the stabilization effect as a result of the delocalization of electron density arising from bonding or lone pair to deficient orbital.⁵⁸ For each Donor (*i*) and Acceptor (*j*) NBOs, the stabilization energy can be defined in terms of the second-order perturbation energy (E^2). Basically, the higher the stabilization energy, the greater the interaction existing between the Donor (*i*) and Acceptor (*j*) orbitals.⁵⁹ The second-order perturbation energy for determining the stability of the studied complexes is generally derived from the mathematical expression in eq 8:

$$E^{(2)} = \Delta E_{i,j} = qi \frac{F^2(i,j)}{E(-E)} \quad (8)$$

From eq 8, the parameter *q* represents donor occupancy, E_i and E_j represent diagonal elements, and $F(i,j)$ represents an element in the Fock matrix. The second-order perturbation energy (E^2) of the donor (*i*) and acceptor (*j*) interacting NBOs within the studied complexes is depicted in Table 3. From this result, only four transitions were dominant in the complexes, including charge transfer from bonding natural orbital of sigma type to antibonding character of lone pair ($\sigma \rightarrow \text{LP}^*$), from antibonding character of lone pairs to antibonding natural orbital of sigma type ($\text{LP}^* \rightarrow \sigma^*$), from lone pair, to center antibonding ($\text{LP} \rightarrow \pi^*$), and finally from the antibonding natural orbital of sigma type to the antibonding natural orbital of sigma type ($\sigma^* \rightarrow \sigma^*$). For the **R2** complex, the intramolecular hyperconjugative interactions with the transition from bonding natural orbital of sigma type between Re and N atoms to the anti-bonding character of lone pair of Re atom [$\sigma\text{Re}_1\text{--N}_{18} \rightarrow \text{LP}^*\text{Re}_1$] was observed to have perturbation energy of 92.94 kcal/mol.

For the **R1**, **R2**, **R3**, **R4**, **R5**, **R6**, **R7**, and **R8** complexes, the perturbation energy values of 92.94, 88.67, 235.3067, 96.7967, 678.4467, 94.7667, 132.2467, and 93.6067 kcal/mol respectively have been obtained. The charge transfers the charge delocalization from the lone pair of the carbon atom (C_3) to the π^* (anti pi) NBO between the Re metal atom and a nitrogen atom. Based on this analysis, it is ostensible that **R5** exhibited the highest second-order perturbation energy which is in tandem with the results from DFT calculations which disclosed that **R5** had the least energy gap and hence, greater reactivity. This is also an indication that **R5** as well as other

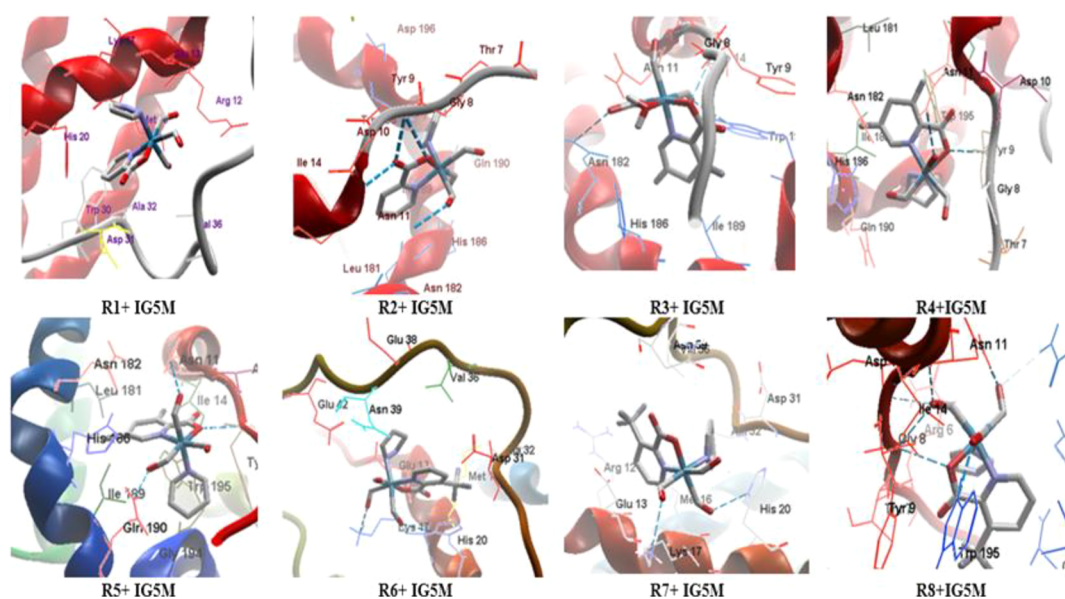


Figure 3. 3D representation of rhenium complexes interaction with ISOFORM 1 of anti-apoptotic HUMAN BCL-2 protein (IGSM) indicating the amino.

complexes might bind favorably with cancer cells and caused significant alterations in the normal metabolic functions of the cells which might induce death or prevent further development. Therefore, **R5** is the most stable complex, exhibiting the transition of LP $C_3 \rightarrow \pi^*Re_1-N_{18}$.

3.3.4. Topology Analysis. The QTAIM, sometimes referred to as the atoms-in-molecule (AIM) hypothesis, gives more insight into the inter and intramolecular interactions of the complexes.⁵⁹ QTAIM analysis is a model developed by Richard F. W. Bader and his research team,⁶⁰ which studies molecular and condensed matter electronic systems and the main object of molecular structure, which is the atoms and bonds.⁶¹ The atoms and their bonds are innate expressions of the electron density distribution function observed in systems.⁶² This model essentially attempts to define bonding in atoms through topological analysis of electron density distribution function.⁶³ QTAIM analysis utilizes the topological parameters such as electron density $\rho(r)$, Laplacian of electron density $\nabla^2\rho(r)$, Lagrangian kinetic energy $G(r)$, Hamiltonian kinetic energy $K(r)$, electronic charge density $V(r)$, and energy density $H(r)$ at critical points (CPs) which are presented in Table S4. To gain more insights into the noncovalent nature of interactions, the AIM hypothesis has proven useful and reliable in DFT study. According to this theory, the structures of molecules are revealed by the critical points of the electron density, alongside the gradient path, which originates and terminates at these points.⁶⁴ The QTAIM model has been judiciously used in this present study to study the bond critical points of the rhenium complexes' inter- and intra-molecular hydrogen bonds, as represented in Table S4. The critical point values were taken for six bonds of each rhenium complex. The values of $\rho(r)$ and $\nabla^2\rho(r)$ are positive and less than one; other topological parameters are also less than one. This implies the accumulation of electron density between two bounded atoms.⁶⁵ The Laplacian of electron density is observed to have a degree of closeness in the values for each bond in all the rhenium complexes. The studied system can be classified into noncovalent, partial covalent, and strongly covalent by using the expression $\nabla^2\rho(r)$ and $H(r)$, combining as: $\nabla^2\rho(r) > 0$ and

$H(r) > 0$; $\nabla^2\rho(r) > 0$ and $H(r) < 0$; and $\nabla^2\rho(r) < 0$ and $H(r) < 0$ identifying the noncovalent, partial covalent, and covalent respectively.⁶⁶ Comparatively, among the six bond critical points of each of the **R1**, **R2**, **R4**, **R5**, **R6**, **R7**, and **R8** complexes, with a close look at the laplacian of electron density, it is observed that $\nabla^2\rho(r) > 0$ and $H(r) < 0$. It is an indication of the presence of a partial covalent interaction. Alternatively, the **R3** complex underwent noncovalent interaction with $\nabla^2\rho(r) > 0$ and $H(r) > 0$ with values of 0.2553 and 0.1433 a.u. respectively. To further inquire into the nature of interactions, $G(r)/V(r)$ and λ_1/λ_3 have been computed, calculated, and presented in Table S3 with the Supporting Information. Note that λ_1/λ_3 defines the bond path softness and higher values designate higher QTAIM softness.⁶⁷ One can clearly see that the λ_1/λ_3 values are observed to be less than one, indicating the strong presence of intermolecular interactions. The ellipticity of electron density (ϵ) has been invoked to gain more insights into the regions of charge density accumulation and the stability of the bond. The ϵ values describe the stability of hydrogen bonds in the different systems. The lower the ellipticity index value, the greater the stability of the complex and vice versa.⁶⁸ The ellipticity index from the QTAIM analysis shows that **R4**, **R6**, **R1**, and **R8** complexes have greater ellipticity index values. This is an indication of the presence of charge transfer and the stability of the complex.

3.4. Molecular Docking Analysis. This analysis was conducted to evaluate the potential of rhenium complexes to disrupt BCL-2 proteins which are the family of proteins that controls an essential step in the prevention of cell apoptosis. These proteins function by regulating the permeabilization of the mitochondrial outer membrane (MOM) as well as the cytoplasm. These proteins cause a dynamic change in conformations that modulate apoptosis in cells. These are often classified as multiregional proapoptotic proteins which are associated with the direct permeabilization of MOM, another class is the BH3 which directly or indirectly activates the pore-forming class members, and the antiapoptotic proteins that inhibit apoptosis at several steps.⁶⁹ The efficacy

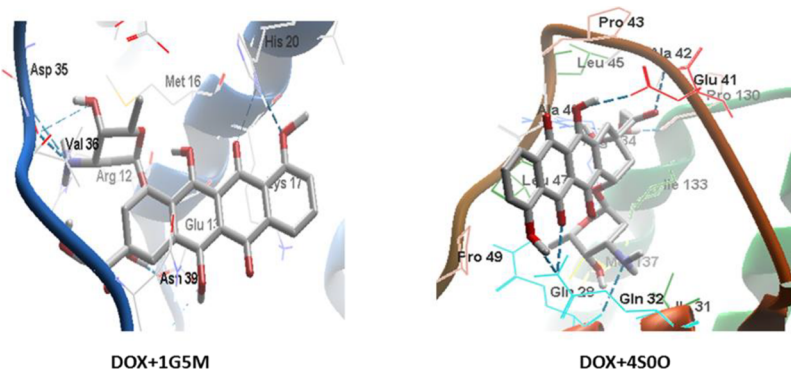


Figure 4. Visualizing the 3D representation of the standard drug with the selected proteins: DOX+1G5M and DOX+4S0O.

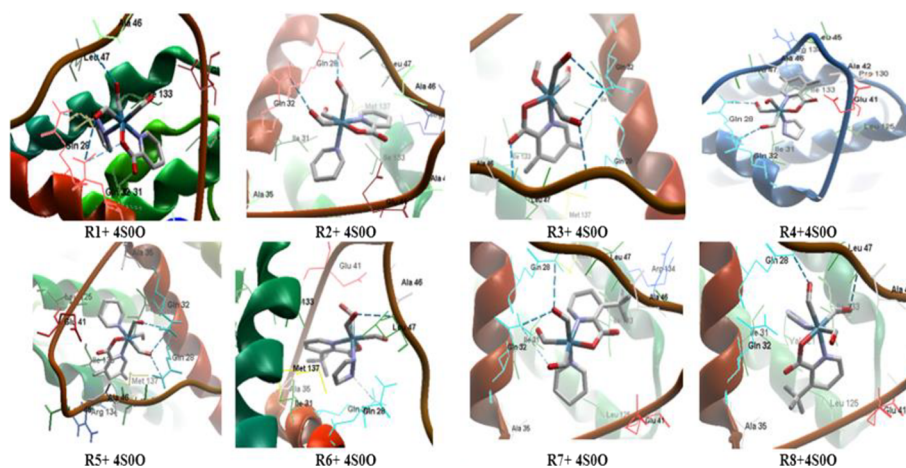


Figure 5. 3D representation of Rhenium complex with pro-apoptotic BAX I protein (4S0O).

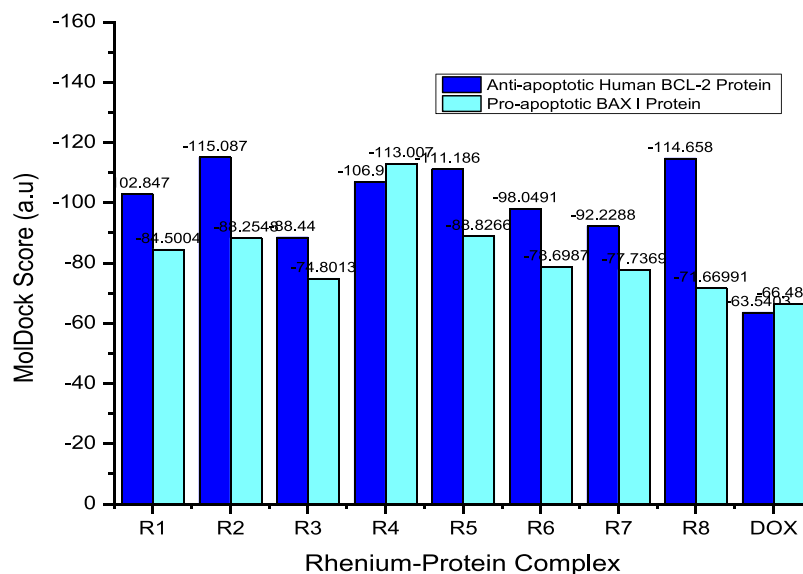


Figure 6. Comparison of MolDock Score of Rhenium complexes with Anti-apoptotic human BCL-2 and pro-apoptotic BAX-1 protein.

of the complexes to inhibit these proteins is investigated via *in silico* computations. Specifically, the antiapoptotic Bcl-2 protein (1G5M) and the proapoptotic derivative (BAX 1, pdb: 4S0O) were selected for docking experiments.^{70,71} The rhenium complex's activity is measured by its propensity to fit into the receptor protein cavity and bind significantly with amino acid residues in the active site. The results of the

docking experiments are tabulated in S4a of Supporting Information and in Figures 3456. The docking results generally disclosed that all the tested metal complexes possess good binding energies with the studied inhibitors. The binding affinity of the complexes with Ig5m receptor was found to be between -3.25 and -10.16 kcal/mol. These energies affirmed that the complexes interacted much favorably with the receptor

than with 4S0O. It is found that the binding affinities of the complexes with the 4S0O receptor are within the range of -2.61 to -6.23 kcal/mol. These binding affinities are quite lower than those found for Ig5m, due to steric repulsions and unfavorable hydrophobic contacts. A careful observation of the type of interactions with which each complex displayed within the respective binding pockets of the receptor shows that more hydrogen bond contacts were persistent between the metal complexes and Ig5m receptor. Typically, hydrogen bond contacts were observed between Asn-10, Asn-11, Asn-182, Trp-195, and Tyr-9 amino acid residues with the complexes. Also, positive steric interactions and electrostatic interactions were observed to stabilize the complexes within the respective binding pockets. These interactions were found between Ala-32, His-20, Lys-17, and Met-16 amino acids residues. Based on these observations, we can conclude that the studied Re complexes are good candidates for disrupting the activities of human BCL-2 proteins, as such, effective in cancer therapy.

4. CONCLUSIONS

DFT computations have been performed to properly evaluate the potency of metal-based rhenium tricarbonyl complexes as inhibitors of human BCL-2 proteins. The results demonstrate that the complexes could substantially alter the regular activities of the BCL class of proteins by binding favorably with the respective proteins. The results from DFT calculations evinced that the complexes are stable. However, **R1** and **R8** were found to be more stable based on energy gap considerations. The values for their energy gaps were found to be 4.0561 and 3.9941 eV respectively. While the metal complexes displayed good reactivity index, **R5** was found to be relatively reactive based on its lower energy gap. The increased reactivity of **R5** was seen to be manifested by its second-order stabilization energy. Moreover, all the metal complexes were found to exhibit high stabilization energy and therefore, suggested that these complexes could bind with the studied proteins to a greater extent. In furtherance, the intermolecular interactions persistent within the metal complexes were unveiled by the QTAIM hypothesis. The results disclosed that intermolecular interactions existed within the complexes and facilitated charge transfers between the ligand and metal centers, thus, stabilizing the complexes. Finally, the results of *in silico* molecular docking investigations are promising and divulged that the complexes could act as good candidates for the development of therapeutic antagonist of BCL class of proteins.

■ ASSOCIATED CONTENT

SI Supporting Information

The Supporting Information is available free of charge at <https://pubs.acs.org/doi/10.1021/acsomega.2c07779>.

Tables S1 and S2 of the Supporting Information shows a comparison of the experimental and theoretical bond length of the most stable complex **R8**, whereas Table S3 presents the tabular representation of QTAIM topology analysis of electron distribution function for **R1–R8**. Finally, Tables S4a and S4b illustrate the docking results of the studied rhenium complexes (PDF)

■ AUTHOR INFORMATION

Corresponding Author

Amanda-Lee E. Manicum – Department of Chemistry, Tshwane University of Technology, Pretoria 0001, South Africa; orcid.org/0000-0003-4064-1307; Email: ManicumAE@tut.ac.za

Authors

Mabu L. Matlou – Department of Chemistry, Tshwane University of Technology, Pretoria 0001, South Africa
Hitler Louis – Computational and Bio-Simulation Research Group, University of Calabar, Calabar 540211, Nigeria
Destiny E. Charlie – Computational and Bio-Simulation Research Group, University of Calabar, Calabar 540211, Nigeria
Ernest C. Agwamba – Computational and Bio-Simulation Research Group, University of Calabar, Calabar 540211, Nigeria; Department of Chemistry, Covenant University, Ota 50001, Nigeria; orcid.org/0000-0002-8008-9572
Ismail O. Amodu – Computational and Bio-Simulation Research Group, University of Calabar, Calabar 540211, Nigeria
Vuyelwa J. Tembu – Department of Chemistry, Tshwane University of Technology, Pretoria 0001, South Africa

Complete contact information is available at:

<https://pubs.acs.org/10.1021/acsomega.2c07779>

Author Contributions

A.-L.E.M.: Conceptualization, review, design, resources, and supervision. V.J.T.: Design, review, resources, and supervision. M.M.: Writing, editing, and manuscript draft. H.L.: Project administrator, analysis, review, and proofreading. E.C.A.: Analysis, writing, and editing. D.C. and I.O.A.: Analysis, writing, and editing.

Funding

The authors would like to thank the National Research Foundation (Grant No. 129468), Tshwane University of Technology, South Africa, for institutional and financial support.

Notes

The authors declare no competing financial interest.

■ ACKNOWLEDGMENTS

The authors would like to acknowledge the center for high-performance computing (CHPC) at the University of Johannesburg, South Africa, for providing computational resources for this research project.

■ REFERENCES

- (1) Abtahi, N. A.; Naghib, S. M.; Ghalekohneh, S. J.; Mohammadpour, Z.; Nazari, H.; Mosavi, S. M.; Gheibihayat, S. M.; Haghirsadat, F.; Reza, J. Z.; Doulabi, B. Z. Multifunctional stimuli-responsive niosomal nanoparticles for co-delivery and co-administration of gene and bioactive compound: In vitro and in vivo studies. *Chem. Eng. J.* **2022**, *429*, No. 132090.
- (2) Srivastava, A.; Patel, H.; Jang, T.; Singer, E.; Ghodoussipour, S. HF02-10 MEDICAL METALS: A BIOGRAPHY OF CISPLATIN. *J. Urol.* **2022**, *207*, No. e209.
- (3) Famurewa, A. C.; Mukherjee, A. G.; Wanjari, U. R.; Sukumar, A.; Murali, R.; Renu, K.; Vellingiri, B.; Dey, A.; Valsala Gopalakrishnan, A. Repurposing FDA-approved drugs against the toxicity of platinum-based anticancer drugs. *Life Sci.* **2022**, *305*, No. 120789.

- (4) Zhang, C.; Xu, C.; Gao, X.; Yao, Q. Platinum-based drugs for cancer therapy and anti-tumor strategies. *Theranostics* **2022**, *12*, 2115–2132.
- (5) Fotopoulou, E.; Titilas, I.; Ronconi, L. Metallo drugs as Anticancer Chemotherapeutics and Diagnostic Agents: A Critical Patent Review (2010–2020). *Recent Pat. Anti-Cancer Drug Discovery* **2022**, *17*, 42–54.
- (6) Peña, Q.; Wang, A.; Zaremba, O.; Shi, Y.; Scheeren, H. W.; Metselaer, J. M.; Kiessling, F.; Pallares, R. M.; Wuttke, S.; Lammers, T. Metallo drugs in cancer nanomedicine. *Chem. Soc. Rev.* **2022**, *51*, 2544–2582.
- (7) Ma, L.; Li, L.; Zhu, G. Platinum-containing heterometallic complexes in cancer therapy: advances and perspectives. *Inorg. Chem. Front.* **2022**, *9*, 2424–2453.
- (8) Meenakshi; Kanaoujiya, R.; Srivastava, S.; Singh, R.; Mustafa, G. Recent advances and application of ruthenium complexes in tumor malignancy. *Mater. Today: Proc.* **2023**, *72*, 2822–2827.
- (9) Wang, Z.; Li, J.; Lin, G.; He, Z.; Wang, Y. Metal complex-based liposomes: Applications and prospects in cancer diagnostics and therapeutics. *J. Controlled Release* **2022**, *348*, 1066–1088.
- (10) Wu, Y.; Li, S.; Chen, Y.; He, W.; Guo, Z. Recent advances in noble metal complex based photodynamic therapy. *Chem. Sci.* **2022**, *13*, 5085–5106.
- (11) Manicum, A.; Schutte-Smith, M.; Kemp, G.; Visser, H. G. Illustration of the electronic influence of coordinated β -diketone type ligands: A kinetic and structural study. *Polyhedron* **2015**, *85*, 190–195.
- (12) Manicum, A.-L. E.; Schutte-Smith, M.; Alexander, O. T.; Twigge, L.; Roodt, A.; Visser, H. G. First kinetic data of the CO substitution in fac-[Re(L,L'-Bid)(CO)₃(X)] complexes (L,L'-Bid = acetylacetonate or tropolonate) by tertiary phosphines PTA and PPh₃: Synthesis and crystal structures of water-soluble rhenium(I) triand dicarbonyl complexes with 1,3,5-triaza-7-phosphaadamantane (PTA). *Inorg. Chem. Commun.* **2019**, *101*, 93–98.
- (13) Manicum, A.-L. E.; Schutte-Smith, M.; Visser, H. G. The synthesis and structural comparison of fac-[Re(CO)₃]⁺ containing complexes with altered β -diketone and phosphine ligands. *Polyhedron* **2018**, *145*, 80–87.
- (14) Sharma, S. A.; Vaibhavi, N.; Kar, B.; Das, U.; Paira, P. Target-specific mononuclear and binuclear rhenium(i) tricarbonyl complexes as upcoming anticancer drugs. *RSC Adv.* **2022**, *12*, 20264–20295.
- (15) Bansal, A.; Saleh-E-In, M. M.; Kar, P.; Roy, A.; Sharma, N. R. Synthesis of Carvacrol Derivatives as Potential New Anticancer Agent against Lung Cancer. *Molecules* **2022**, *27*, 4597.
- (16) Knopf, K. M.; Murphy, B. L.; MacMillan, S. N.; Baskin, J. M.; Barr, M. P.; Boros, E.; Wilson, J. J. In Vitro Anticancer Activity and in Vivo Biodistribution of Rhenium(I) Tricarbonyl Aqua Complexes. *J. Am. Chem. Soc.* **2017**, *139*, 14302–14314.
- (17) Suárez-Ortiz, G. A.; Hernández-Correa, R.; Morales-Moreno, M. D.; Toscano, R. A.; Ramirez-Apan, M. T.; Hernandez-García, A.; Amézquita-Valencia, M.; Araza-Olivera, D. Diastereomeric Separation of Chiral fac-Tricarbonyl(iminopyridine) Rhenium(I) Complexes and Their Cytotoxicity Studies: Approach toward an Action Mechanism against Glioblastoma. *J. Med. Chem.* **2022**, *65*, 9281–9294.
- (18) Wiratpruk, N.; Bindra, G. K.; Hamilton, A.; Hulett, M. D.; Barnard, P. J. Cytotoxic properties of rhenium(i) tricarbonyl complexes of N-heterocyclic carbene ligands. *Dalton Trans.* **2022**, *51*, 7630–7643.
- (19) Collery, P.; Desmaele, D.; Vijaykumar, V. Design of Rhenium Compounds in Targeted Anticancer Therapeutics. *Curr. Pharm. Des.* **2019**, *25*, 3306–3322.
- (20) Vente, M. A.; Hobbelink, M. G.; van Het Schip, A. D.; Zonnenberg, B. A.; Nijsen, J. F. Radionuclide liver cancer therapies: from concept to current clinical status. *Anti-Cancer Agents Med. Chem.* **2007**, *7*, 441–459.
- (21) Patra, M.; Gasser, G. The medicinal chemistry of ferrocene and its derivatives. *Nat. Rev. Chem.* **2017**, *1*, No. 0066.
- (22) Eno, E. A.; Louis, H.; Ekoja, P.; Benjamin, I.; Adalikwu, S. A.; Orosun, M. M.; Unimuke, T. O.; Asogwa, F. C.; Agwamba, E. C. Experimental and computational modeling of the biological activity of benzaldehyde sulphur trioxide as a potential drug for the treatment of Alzheimer disease. *J. Indian Chem. Soc.* **2022**, *99*, No. 100532.
- (23) Wei, K.; Louis, H.; Emori, W.; Idante, P. S.; Agwamba, E. C.; Cheng, C.-R.; Eno, E. A.; Unimuke, T. O. Antispasmodic activity of carnosic acid extracted from *rosmarinus officinalis*: Isolation, spectroscopic characterization, DFT studies, and in silico molecular docking investigations. *J. Mol. Struct.* **2022**, *1260*, No. 132795.
- (24) Eno, E. A.; Patrick-Inezi, F. A.; Louis, H.; Gber, T. E.; Unimuke, T. O.; Agwamba, E. C.; Ikenyirimba, O. J.; Akpanke, J. A.; Oyoita, E.; Ejiofor, E. U.; Adalikwu, S. A. Theoretical investigation and antineoplastic potential of Zn (II) and Pd (II) complexes of 6-methylpyridine-2-carbaldehyde-N (4)-ethylthiosemicarbazone. *Chem. Phys. Impact* **2022**, *5*, No. 100094.
- (25) Agwamba, E. C.; Udoikono, A. D.; Louis, H.; Udoh, E. U.; Benjamin, I.; Igbalagh, A. T.; Edet, H. O.; Ejiofor, E. U.; Ushaka, U. B. Synthesis, characterization, DFT studies, and molecular modeling of azo dye derivatives as potential candidate for trypanosomiasis treatment. *Chem. Phys. Impact* **2022**, *4*, No. 100076.
- (26) Asogwa, F. C.; Agwamba, E. C.; Louis, H.; Muozie, M. C.; Benjamin, I.; Gber, T. E.; Mathias, G. E.; Adeyinka, A. S.; Ikeuba, A. I. Structural benchmarking, density functional theory simulation, spectroscopic investigation and molecular docking of N-(1H-pyrrol-2-yl) methylene)-4-methylaniline as castration-resistant prostate cancer chemotherapeutic agent. *Chem. Phys. Impact* **2022**, *5*, No. 100091.
- (27) Franco, J. H.; da Silva, B. F.; Dias, E. F. G.; de Castro, A. A.; Ramalho, T. C.; Zanoni, M. V. B. Influence of auxochrome group in disperse dyes bearing azo groups as chromophore center in the biotransformation and molecular docking prediction by reductase enzyme: Implications and assessment for environmental toxicity of xenobiotics. *Ecotoxicol. Environ. Saf.* **2018**, *160*, 114–126.
- (28) Radaeva, M.; Dong, X.; Cherkasov, A. The Use of Methods of Computer-Aided Drug Discovery in the Development of Topoisomerase II Inhibitors: Applications and Future Directions. *J. Chem. Inf. Model.* **2020**, *60*, 3703–3721.
- (29) Reddy, R. N.; Mutyala, R.; Aparoy, P.; Reddanna, P.; Reddy, M. R. Computer aided drug design approaches to develop cyclooxygenase based novel anti-inflammatory and anti-cancer drugs. *Curr. Pharm. Des.* **2007**, *13*, 3505–3517.
- (30) Elkaeed, E. B.; Yousef, R. G.; Elkady, H.; Gobaara, I. M. M.; Alsfouk, A. A.; Husein, D. Z.; Ibrahim, I. M.; Metwaly, A. M.; Eissa, I. H. The Assessment of Anticancer and VEGFR-2 Inhibitory Activities of a New 1H-Indole Derivative: In Silico and In Vitro Approaches. *Processes* **2022**, *10*, 1391.
- (31) Saeed, A. M.; AlNeyadi, S. S.; Abdou, I. M. Anticancer activity of novel Schiff bases and azo dyes derived from 3-amino-4-hydroxy-2H-pyran[3,2-c]quinoline-2,5(6H)-dione. *Heterocycl. Commun.* **2020**, *26*, 192–205.
- (32) Khattab, M.; Al-Karmalawy, A. A. Revisiting Activity of Some Nocardazole Analogues as a Potential Anticancer Drugs Using Molecular Docking and DFT Calculations. *Front. Chem.* **2021**, No. 628398.
- (33) Al-Otaibi, J. S.; Ullah, Z.; Mary, Y. S.; Mary, Y. S.; Soman, S.; Thirunavukkarasu, M.; Kwon, H. W. DFT investigations on conformational analysis, solvation effects, reactivity studies, chemical descriptors and docking of two anti-cancerous drugs, Lenvatinib and Regorafenib. *Vietnam J. Chem.* **2022**, *60*, 636.
- (34) Murphy, B. L.; Marker, S. C.; Lambert, V. J.; Woods, J. J.; MacMillan, S. N.; Wilson, J. J. Synthesis, characterization, and biological properties of rhenium(I) tricarbonyl complexes bearing nitrogen-donor ligands. *J. Organomet. Chem.* **2020**, *907*, No. 121064.
- (35) Mkhathshwa, M.; Moremi, J. M.; Makgopa, K.; Manicum, A. E. Nanoparticles Functionalised with Re(I) Tricarbonyl Complexes for Cancer Theranostics. *Int. J. Mol. Sci.* **2021**, *22*, 6546.
- (36) Matlou, M. L.; Malan, F. P.; Nkadameng, S.; McGaw, L.; Tembu, V. J.; Manicum, A.-L. E. Exploring the in vitro anticancer activities of Re(I) picolinic acid and its fluorinated complex

- derivatives on lung cancer cells: a structural study. *J. Biol. Inorg. Chem.* **2022**, DOI: 10.1007/s00775-022-01971-2.
- (37) Manicum, A.-L. E.; Schutte-Smith, M.; Malan, F. P.; Visser, H. G. Steric and electronic influence of Re(I) tricarbonyl complexes with various coordinated β -diketones. *J. Mol. Struct.* **2022**, 1264, No. 133278.
- (38) Moherane, L.; Alexander, O. T.; Visser, H. G.; Manicum, A.-L. E. The crystal structure of [μ -hydroxido-bis[(5,5'-dimethyl-2,2'-bipyridine- κ 2N,N')-tricarbonylrhenium(I)] bromide hemihydrate, C₃₀H₂₆N₄O₉Re₂Br. *Z. Kristallogr. - New Cryst. Struct.* **2021**, 236, 1027–1029.
- (39) Manicum, A.-L.; Alexander, O.; Schutte-Smith, M.; Visser, H. G. Synthesis, characterization and substitution reactions of fac-[Re(O,O'-bid)(CO)₃(P)] complexes, using the “2+1” mixed ligand model. *J. Mol. Struct.* **2020**, 1209, No. 127953.
- (40) Goedecker, S.; Hellmann, W.; Lenosky, T. Global Minimum Determination of the Born-Oppenheimer Surface within Density Functional Theory. *Phys. Rev. Lett.* **2005**, 95, No. 055501.
- (41) Nemykin, V. N.; Hadt, R. G.; Belosludov, R. V.; Mizuseki, H.; Kawazoe, Y. Influence of molecular geometry, exchange-correlation functional, and solvent effects in the modeling of vertical excitation energies in phthalocyanines using time-dependent density functional theory (TDDFT) and polarized continuum model TDDFT methods: can modern computational chemistry methods explain experimental controversies? *J. Phys. Chem. A* **2007**, 111, 12901–12913.
- (42) Truong, H. B.; Huy, B. T.; Ray, S. K.; Gyawali, G.; Lee, Y. I.; Cho, J.; Hur, J. Magnetic visible-light activated photocatalyst ZnFe(2)O(4)/BiVO(4)/g-C(3)N(4) for decomposition of antibiotic lomefloxacin: Photocatalytic mechanism, degradation pathway, and toxicity assessment. *Chemosphere* **2022**, 299, No. 134320.
- (43) Liao, X.; Lu, R.; Xia, L.; Liu, Q.; Wang, H.; Zhao, K.; Wang, Z.; Zhao, Y. Density Functional Theory for Electrocatalysis. *Energy Environ. Mater.* **2022**, 5, 157–185.
- (44) Doust Mohammadi, M.; Abdullah, H. Y.; Bhowmick, S.; Biskos, G. Silicon Carbide Based Nanotubes as a Sensing Material for Gaseous H₂SiCl₂. *Silicon* **2023**, 15, 177.
- (45) Petros, A. M.; Medek, A.; Nettesheim, D. G.; Kim, D. H.; Yoon, H. S.; Swift, K.; Matayoshi, E. D.; Oltersdorf, T.; Fesik, S. W. Solution structure of the antiapoptotic protein bcl-2. *Proc. Natl. Acad. Sci. U. S. A.* **2001**, 98, 3012–3017.
- (46) Garner, T. P.; Reyna, D. E.; Priyadarshi, A.; Chen, H. C.; Li, S.; Wu, Y.; Ganesan, Y. T.; Malashkevich, V. N.; Cheng, E. H.; Gavathiotis, E. An Autoinhibited Dimeric Form of BAX Regulates the BAX Activation Pathway. *Mol. Cell* **2016**, 63, 485–497.
- (47) Chen, Y.; Ma, J.; Wang, F.; Hu, J.; Cui, A.; Wei, C.; Yang, Q.; Li, F. Amygdalin induces apoptosis in human cervical cancer cell line HeLa cells. *Immunopharmacol. Immunotoxicol.* **2013**, 35, 43–51.
- (48) Mayer, D. M.; Tonge, C. M.; Nguyen, G. D.; Hojo, R.; Paisley, N. R.; Yu, J.; Tom, G.; Burke, S. A.; Hudson, Z. M. Design of High-Performance Thermally Activated Delayed Fluorescence Emitters Containing s-Triazine and s-Heptazine with Molecular Orbital Visualization by STM. *Chem. Mater.* **2022**, 34, 2624–2635.
- (49) Jaziri, E.; Louis, H.; Gharbi, C.; Unimuke, T. O.; Agwamba, E. C.; Mathias, G. E.; Fugita, W.; Nasr, C. B.; Khedhiri, L. Synthesis, X-ray crystallography, molecular electronic property investigation, and leukopoiesis activity of novel 4,6-dimethyl-1,6-dihydropyridin-2-amino nitrate hybrid material. *J. Mol. Struct.* **2022**, 1268, No. 133733.
- (50) Shmilovich, K.; Yao, Y.; Tovar, J. D.; Katz, H. E.; Schleife, A.; Ferguson, A. L. Computational discovery of high charge mobility self-assembling π -conjugated peptides. *Mol. Syst. Des. Eng.* **2022**, 7, 447–459.
- (51) Islam, M. R.; Awal, M. A.; Khames, A.; Abourehab, M. A. S.; Samad, A.; Hassan, W. M. I.; Alam, R.; Osman, O. I.; Nur, S. M.; Molla, M. H. R.; Abdulrahman, A. O.; Rajia, S.; Ahammad, F.; Hasan, M. N.; Qadri, I.; Kim, B. Computational Identification of Druggable Bioactive Compounds from Catharanthus roseus and Avicennia marina against Colorectal Cancer by Targeting Thymidylate Synthase. *Molecules* **2022**, 27, 2089.
- (52) Zhang, T.; Svensson, P. H. W.; Brumboiu, I. E.; Lanzilotto, V.; Grazioli, C.; Guarnaccio, A.; Johansson, F. O. L.; Beranová, K.; Coreno, M.; de Simone, M.; Floreano, L.; Cossaro, A.; Brena, B.; Puglia, C. Clarifying the Adsorption of Triphenylamine on Au(111): Filling the HOMO–LUMO Gap. *J. Phys. Chem. C* **2022**, 126, 1635–1643.
- (53) Yang, J.; Chen, X.; Liu, Z.; Wang, Q.; Wen, Y.; Zhang, A.; Chen, R.; Shan, B. Theoretical design principles of metal catalysts for selective ammonia oxidation from high throughput computation. *J. Mater. Chem. A* **2022**, 10, 12447–12457.
- (54) Alhomrani, M.; Alsanie, W. F.; Alamri, A. S.; Alyami, H.; Habeebullah, H.; Alkhatabi, H. A.; Felimban, R. I.; Haynes, J. M.; Shakya, S.; Raafat, B. M.; Refat, M. S.; Gaber, A. Enhancing the Antipsychotic Effect of Risperidone by Increasing Its Binding Affinity to Serotonin Receptor via Picric Acid: A Molecular Dynamics Simulation. *Pharmaceuticals* **2022**, 15, 285.
- (55) Bano, R.; Hussain, S.; Arshad, M.; Rauf, A.; Mahmood, T.; Ayub, K.; Gilani, M. A. Lanthanum doped corannulenes with enhanced static and dynamic nonlinear optical properties: A first principle study. *Phys. B* **2022**, 641, No. 414088.
- (56) Jayashankar, J.; Hema, M. K.; Mahmoudi, G.; Masoudiasl, A.; Dušek, M.; Montazerzohori, M.; Karthik, C. S.; Lokanath, N. K. N,N'-bis(2-bromobenzylidene)-2,2'-diaminodiphenyldisulfide (BBDD): Insights of crystal structure, DFT, QTAIM, PASS, ADMET and molecular docking studies. *J. Mol. Struct.* **2022**, 1268, No. 133657.
- (57) Raja, M.; Raj Muhamed, R.; Muthu, S.; Suresh, M. Synthesis, spectroscopic (FT-IR, FT-Raman, NMR, UV–Visible), NLO, NBO, HOMO-LUMO, Fukui function and molecular docking study of (E)-1-(5-bromo-2-hydroxybenzylidene)semicarbazide. *J. Mol. Struct.* **2017**, 1141, 284–298.
- (58) Benjamin, I.; Udoikono, A. D.; Louis, H.; Agwamba, E. C.; Unimuke, T. O.; Owen, A. E.; Adeyinka, A. S. Antimalarial potential of naphthalene-sulfonic acid derivatives: Molecular electronic properties, vibrational assignments, and in-silico molecular docking studies. *J. Mol. Struct.* **2022**, 1264, No. 133298.
- (59) Barker, J. A.; Henderson, D. Perturbation Theory and Equation of State for Fluids. II. A Successful Theory of Liquids. *J. Chem. Phys.* **1967**, 47, 4714–4721.
- (60) Zhang, N.-N.; Li, J.; Xiao, H. The Key Role of Competition between Orbital and Electrostatic Interactions in the Adsorption on Transition Metal Single-Atom Catalysts Anchored by N-doped Graphene. *ChemCatChem* **2022**, 14, No. e202200275.
- (61) Di Sabatino, S.; Koskelo, J.; Berger, J. A.; Romaniello, P. Introducing screening in one-body density matrix functionals: Impact on charged excitations of model systems via the extended Koopmans' theorem. *Phys. Rev. B* **2022**, 105, No. 235123.
- (62) Cukrowski, I. A unified molecular-wide and electron density based concept of chemical bonding. *WIREs Comput. Mol. Sci.* **2022**, 12, No. e1579.
- (63) Eno, E. A.; Louis, H.; Unimuke, T. O.; Gber, T. E.; Mbonu, I. J.; Ndubisi, C. J.; Adalikwu, S. A. Reactivity, stability, and thermodynamics of para-methylpyridinium-based ionic liquids: Insight from DFT, NCI, and QTAIM. *J. Ionic Liq.* **2022**, 2, No. 100030.
- (64) Louis, H.; Amodu, I. O.; Unimuke, T. O.; Gber, T. E.; Isang, B. B.; Adeyinka, A. S. Modeling of Ca12O12, Mg12O12, and Al12N12 nanostructured materials as sensors for phosgene (Cl₂CO). *Mater. Today Commun.* **2022**, 32, No. 103946.
- (65) Rafiq, M.; Salim, M.; Noreen, S.; Ahmad Khara, R.; Noor, S.; Yaqoob, U.; Iqbal, J. End-capped modification of dithienosilole based small donor molecules for high performance organic solar cells using DFT approach. *J. Mol. Liq.* **2022**, 345, No. 118138.
- (66) Moussa, H.; Bouafia, H.; Sahli, B.; Dorbane, A.; Uğur, Ş.; Uğur, G. Elastic isotropy, magnetic and electronic properties, bonding and non-covalent interactions analyses of HoFe₄P12 filled-skutterudite: DFT + U + SOC, QTAIM and NCI investigations. *J. Magn. Magn. Mater.* **2021**, 518, No. 167435.
- (67) Jenkinsa, S.; Blancafortb, L.; Kirka, S. R.; Bearpark, M. J. The response of the electronic structure to electronic excitation and

double bond torsion in fulvene: a combined QTAIM, stress tensor and Mo perspective. *Phys. Chem. Phys.* **2014**, *16*, 7115–7126.

(68) Fasshauer, D.; Otto, H.; Eliason, W. K.; Jahn, R.; Brünger, A. T. Structural Changes Are Associated with Soluble N-Ethylmaleimide-sensitive Fusion Protein Attachment Protein Receptor Complex Formation*. *J. Biol. Chem.* **1997**, *272*, 28036–28041.

(69) Dennington, R.; Keith, T. A.; Millam, J. M. *GaussView 6.0*. 16; Semichem Inc.: Shawnee Mission, KS, USA, 2016.

(70) HyperChem, T *HyperChem 8.07, HyperChem Professional Program*; Hypercube: Gainesville, 2001.

(71) Shamas-Din, A.; Kale, J.; Leber, B.; Andrews, D. W. Mechanisms of Action of Bcl-2 family proteins. *Cold Spring Harbor Perspect. Biol.* **2013**, *5*, No. a008714.

(72) RCSB PDB. 1G5M: Human BCL-2, Isoform 1; <https://www.rcsb.org/structure/1G5M> 1/3. DOI: 10.2210/pdb1G5M/pdb.

(73) RCSB PDB. 4S0O: Crystal Structure of the Autoinhibited Dimer of Pro-apoptotic BAX (I); <https://www.rcsb.org/structure/4S0O> 1/4. DOI: 10.2210/pdb4S0O/pdb.